Towards Wearable Piezoelectric Energy Harvesting: Modeling and Experimental Validation

Yigit Tuncel
ytuncel@asu.edu

Shiva Bandyopadhyay
sbandyo9@asu.edu

Shambhavi V. Kulshrestha
skulshr5@asu.edu

Audrey Mendez
afmendez@asu.edu

Umit Y. Ogras
umit@asu.edu

ABSTRACT

Motion energy harvesting is an ideal alternative to battery in wearable applications since it can produce energy on demand. So far, widespread use of this technology has been hindered by bulky, inflexible and impractical designs. New flexible piezoelectric materials enable comfortable use of this technology. However, the energy harvesting potential of this approach has not been thoroughly investigated to date. This paper presents a novel mathematical model for estimating the energy that can be harvested from joint movements on the human body. The proposed model is *validated using two different piezoelectric materials* attached on a 3D model of the human knee. To the best of our knowledge, this is *the first study that combines analytical modeling and experimental validation for joint movements*. Thorough experimental evaluations show that 1) users can generate on average 13 μW power while walking, 2) we can predict the generated power with 4.8% modeling error.

CCS CONCEPTS

• **Hardware → Power and energy**.

KEYWORDS

Wearable piezoelectric energy harvesting, joint-bending, mechanical knee-frame, mathematical modeling, experimental validation

1 INTRODUCTION

Advances in low-power electronics and miniaturization have paved the way for many novel wearable devices and applications [1–4]. However, limited battery capacity of such wearable devices has hindered their widespread adoption. This motivated research on wearable energy harvesting as an alternative energy source. With energy harvesting, the device can generate usable electrical energy from various sources in the environment [5]. The most common energy sources for wearable energy harvesting are light, motion, electromagnetic waves, and heat [6]. Among these, motion energy is particularly interesting as it is shown to have a power density as high as 200 μW/cm^2 [5, 7] and is available on demand.
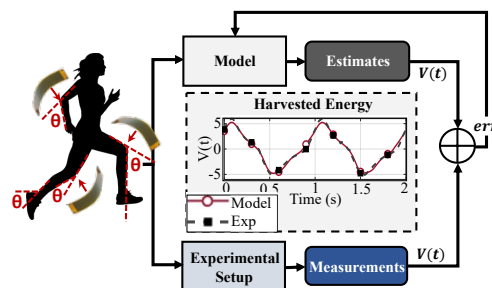
Figure 1: Overview of the modeling and experimental validation of piezoelectric energy harvesting from joint bending.

For example, energy due to human activity will be available when required by activity monitoring applications. Therefore, motion energy harvesting is an ideal energy source for wearable devices.

Motion energy harvesting solutions commonly use piezoelectric materials to transform mechanical energy to electrical voltage. These materials generate maximum power at mechanical resonant frequencies in the order of 100 Hz, which is at least *an order of magnitude larger than the frequency content of human dynamics*. Studies on wearable piezoelectric energy harvesting (PEH) address this by employing frequency up/down-conversion techniques through complex mechanical designs [7–9]. However, these complex designs need to be contained in an external frame worn by the user. Historically, these materials have been inflexible and brittle [10] which further limited their use in wearable applications.

Flexible piezoelectric materials, such as Polyvinylidene Fluoride (PVDF) and Macro-Fiber Composite (MFC), alleviate the bulkiness and inflexibility constraints. Hence, they enable the placement of piezoelectric materials directly on human joints [11]. For example, knees, elbows and ankles are candidate locations for placing these materials as depicted in Figure 1. Despite the promise of this approach to solve comfort concerns, very few studies investigated the energy harvesting potential of flexible piezoelectric patches [11, 12]. Furthermore, these prior studies follow a purely experimental approach and *do not model the energy harvesting mechanism*. A model-based approach is critical for identifying dependencies to parameters in the system and predicting the harvested energy in real-life scenarios. Therefore, there is a strong need for modeling piezoelectric energy harvesting directly from joint bending.

The contributions of this paper are twofold. First, it presents a novel mathematical model for the energy harvesting output of a piezoelectric patch directly placed on the joint. Then, it provides an extensive experimental evaluation that both validates the model

and demonstrates the energy harvesting potential of wearable PEH. Using the proposed model, we show that wearable piezoelectric energy harvesting potential from the knee joint is sufficient to sustain low-power applications. According to our results, users can generate on average 13 μW power while walking. Our evaluations also show that the monthly energy capacity of a person taking 7500 steps/day is equivalent to a 0.40 mAh battery rated at 1.2V.

The major contributions of this work are:

- Mathematical modeling of piezoelectric energy harvesting from low-frequency, large-bending joint movements.
- Experimental evaluation that validates the model and demonstrates the energy potential of wearable PEH.

2 RELATED WORK

Wearable PEH solutions vibrate the piezoelectric material at its mechanical resonance frequency to obtain maximum power [7–9]. Since human motion is in the order of a few Hertz, these approaches up-convert the slow-motion to the resonant frequency using mechanical designs. Consequently, they do not use the large-bending of the joint as their energy source. They also do not leverage the flexibility of the novel materials into their designs. For example, authors in [9] harvest motion energy by attaching eight piezoelectric patches to cantilever beams contained in a circular frame mounted on the leg. Although the generated power is close to 6 mW, the design is bulky and lacks flexible form-factor, which render it impractical for wearable applications, as summarized in Table 1.

Few studies have investigated the energy harvesting potential from directly placing the piezoelectric materials on the joints. Proto et al. [11] place PVDF and MFC patches at various locations on the body. They record the harvested energy during different physical activities, such as walking, jogging and climbing up/down stairs. They report 1.9 μW generated power from walking motion. Another study uses a mechanical frame to explore the dynamics of energy harvesting from human gait [12]. According to their results, close to 1 μW is generated by an MFC patch from walking motion. Although these studies provide useful insight into wearable PEH potential from joint movements, they are purely experimental and *lack the analytical modeling* of the energy harvesting mechanism.

Analytical modeling is very critical as it helps to understand dependencies on various parameters in the system. It also enables realistic energy estimates from a wide array of different motions. Cha [13] provides a theoretical analysis of the power generated from a PVDF patch placed on the human knee. Throughout the analysis, a small-angle approximation for the bending of the piezoelectric patch is used. However, this is inadequate as human joint motions involve large-bending movements. Besides this, the proposed model *is not validated* through experimental measurements.

Table 1: Compilation of recent related work in wearable PEH

Ref	Analytical Model	Experimental Validation	Large Bending	Flexible Form-factor	Reported Power
[9]	✓	✓	✗	✗	6 mW
[11]	✗	✓	✓	✓	1.9 μW
[12]	✗	✓	✓	✓	1.0 μW
[13]	✓	✗	✗	✓	1.0 μW
This Work	✓	✓	✓	✓	**13 μW**

To the best of our knowledge, *this is the first study that combines the modeling and experimental validation of piezoelectric energy harvesting directly from joint movements.* It presents a novel mathematical model for piezoelectric energy harvesting from low-frequency, large-bending joint movements. We validate this model using a 3D printed human knee model. Finally, we use the established model to estimate the energy harvesting potential during walking, further paving the way for wearable piezoelectric energy harvesting.

3 OVERVIEW OF THE PROPOSED APPROACH

We consider a flexible piezoelectric patch that is directly placed on a joint, such as those in Figure 1. The proposed approach consists of three major components: 1) Modeling the physical displacement under *large-bending conditions*, 2) Converting the displacement to voltage, 3) Experimental validation and parameter identification.

1. The joint bending model relates the joint bending angle to strain induced in the piezoelectric patch. It finds the horizontal displacement and curvature of the piezoelectric patch for a given joint movement. Using these, the strain in the piezoelectric patch is calculated, as explained in Section 4.3. This sub-model addresses the large-bending challenge introduced by large joint rotations.

2. The piezoelectricity model expresses the generated voltage according to the induced strain in the piezoelectric patch. It first calculates the accumulated charge in the material. Then, the derivative of charge with respect to time yields the current passing through. Finally, the current flows through the load resistance and determines the voltage across this load and generated power, as explained in Section 4.2. Figure 2 illustrates these modeling steps.

3. Experimental validation is crucial to demonstrate the practical use of the proposed model and identify the values of model parameters. To obtain reliable and repeatable measurements, we removed the human factor by designing a 3D printed bending frame. This setup is used to record the generated voltages from two piezoelectric elements with different dimensions under sinusoidal actuation with different motion frequencies and amplitudes. Finally, the model is further optimized to minimize the error between experimental and modeling results by tuning key parameters in the model, as illustrated in Figure 1. Experimental evaluation and real-life applications scenarios are presented in Section 5.

4 MODELING OF PIEZOELECTRIC ENERGY HARVESTING FROM JOINT MOVEMENT

Electrical forces induced by the piezoelectric material are comparable to the weak mechanical forces *in most piezoelectricity literature* [14], such as vibration. The mechanical and electrical governing equations couple these forces to calculate the mechanical displacement and electrical voltage in the piezoelectric material. In our case, however, the mechanical forces acting on the piezoelectric patch due to large-bending motion are significantly larger than the generated electrical forces. This allows the electrical and mechanical
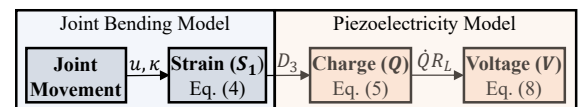

Figure 2: Overview of the proposed modeling approach.

domains to be completely decoupled [15]. Hence, we consider only the electrical governing equation in this study [14]:

$$D_3 = \epsilon_{33}^S E_3^S + e_{31} S_1 \tag{1}$$

where D_3 is the electric displacement field along the thickness of the material. The input to the system is S_1, the strain induced in the piezoelectric material, as summarized in Table 2. In the following, we first find an expression for S_1 as a function of the joint angle (Section 4.3) and combine that expression with Equation 1 to find the generated voltage across the load (Section 4.2).

4.1 Mechanical Joint Bending Model

We use the large-bending representation of a cantilever beam over a circular support as shown in Figure 3. The joint is modeled as a circular profile with a radius r, while the piezoelectric patch is illustrated as a beam that bends along the circular profile according to the joint bend angle θ. The neutral position of the patch is shown with the flat line ①. As joint bends, the patch moves from position ① to ②, taking a curved form.

In the illustration, positions $s = 0$ and $s = L$ show the clamped (i.e., fixed) and free ends of the patch, respectively. The point marked by $s = s_0$ is the first point in contact with the circular profile, while $s = s_1$ is the last point that touches the circle. Using the arc length on the circular profile, we obtain $s_1(t) = s_0 + r\theta(t)$, where $\theta(t)$ is the bending angle. As the piezoelectric patch bends from ① to ②, the points along it exhibit horizontal and vertical displacements, as illustrated in Figure 3. The horizontal displacement of an arbitrary point $u(s, t)$ for $0 \le s \le L$, can be expressed as:

$$u(s, t) = \begin{cases} 0, & 0 \le s \le s_0 \\ s_1(t) - s, & s_0 \le s \le s_1(t) \\ s_0 + r\sin\theta(t) + (L - s_1(t))\cos\theta(t) - s, & s_1(t) \le s \le L \end{cases} \tag{2}$$

The strain on the piezoelectric patch is a function of its curvature, which depends on the vertical displacement $\omega(s, t)$. Due to the circular profile of the joint, the curvature $\kappa(s, t)$ can be written as:

$$\kappa(s, t) = \frac{\frac{\partial^2 \omega(s,t)}{\partial s^2}}{\left(1 + \left(\frac{\partial \omega(s,t)}{\partial s}\right)^2\right)^{\frac{3}{2}}} = \begin{cases} \frac{1}{r}, & s_0 \le s \le s_1(t) \\ 0, & otherwise \end{cases} \tag{3}$$

Table 2: Summary of symbols used in this paper

| Symbol	Parameter	Symbol	Parameter
D_3	Electric displacement field	ϵ_{33}^S	Permittivity under constant strain
V	Generated voltage	Q	Accumulated charge
i	Generated current	A	PZ Area
E_3^S	Electric field	L	PZ Length
S_1	Axial Strain	W	PZ Width
κ	Curvature	C	PZ Capacitance
u	Horz. displacement	R_L	PZ Load
d_{31}	Strain coefficient	Y_p	PZ Young's Modulus
θ	Joint bend angle	h_p	PZ Thickness
ω	Vert. displacement	Y_s	SB Young's Modulus
r	Radius of curvature	h_s	SB Thickness
e_{31}	Electromechanical coupling coefficient [15]	h_{pc}	Distance to neutral axis

PZ: Piezoelectric Patch. SB: Substrate.
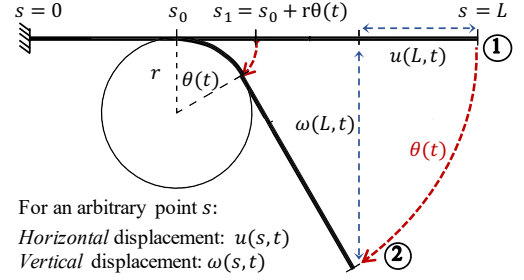
Figure 3: Large-bending representation of the joint

Finally, the strain in the large-bending representation can be found as a function of horizontal displacement and curvature as:

$$S_1(s, t) = -h_{pc}\kappa(s, t) + \frac{\partial u(s, t)}{\partial s} \tag{4}$$

where $h_{pc} = \frac{Y_s h_s (h_p + h_s)}{2(Y_p h_p + Y_s h_s)}$ is the distance to the neutral axis in the thickness direction of the piezoelectric patch [14, 15]. Next, we use this expression to develop the piezoelectricity model that gives the generated voltage due to the induced strain.

4.2 Piezoelectricity Model

The charge accumulated on the piezoelectric patch can be found by applying the Gauss Law to the electric field given in Equation 1:

$$Q(t) = \int_0^W \int_0^L D_3 \, dW \, dL = \int_0^W \int_0^L \left(\epsilon_{33}^S E_3^S(t) + e_{31} S_1(s, t) \right) dW \, dL \tag{5}$$

where W and L denote the width and length of the piezoelectric patch, respectively. Since E_3^S is constant along the area and S_1 is constant along the width of the patch, the integrals simplify to:

$$Q(t) = \epsilon_{33}^S W L E_3^S(t) + e_{31} W \int_0^L S_1(s, t) \, dL \tag{6}$$

Electric field within the piezoelectric layer is given by the ratio of the voltage and thickness of the piezoelectric patch: $E_3^S(t) = -\frac{V(t)}{h_p}$. By substituting the electric field and strain expressions (Equation 4) to Equation 6, the electric charge can be found as:

$$Q(t) = -\frac{\epsilon_{33}^S W L}{h_p} V(t) + e_{31} W \int_0^L \left(-h_{pc}\kappa(s, t) + \frac{\partial u(s, t)}{\partial s} \right) ds \tag{7}$$

The term multiplied with the voltage is referred to as the capacitance of the patch [14], and is denoted by $C = \frac{\epsilon_{33}^S W L}{h_p}$ from here on.

Main Theoretical Result: *The voltage generated by the piezoelectric patch is governed by the following differential equation:*

$$\frac{dV(t)}{dt} = \frac{-V(t)}{R_L C} + \frac{e_{31} W}{C} \left(-h_{pc} \frac{d\theta(t)}{dt} + (s_1(t) - L) \frac{d\theta(t)}{dt} \sin\theta(t) \right) \tag{8}$$

Proof: This equation can be derived by taking the derivative of the expression in Equation 7 and multiplying the result with the load resistance (i.e., $V(t) = \frac{dQ(t)}{dt} R_L$). The step-by-step derivation is given in Appendix A to improve the readability of this section. □

4.3 Fine-tuning Model Parameters

In small-bending problems, horizontal displacement is negligible compared to the length of the patch. Since most studies consider a vibrating beam (i.e. very small-bending), typically all the contribution to voltage comes from the bold highlighted term in Equation 8. However, contributions from both terms are significant for a large-bending problem, as shown for a cantilever beam in [15]. Furthermore, parameter variations, such as the thickness of the material, can affect the accuracy of Equation 8, if we rely only on the datasheet values. To compensate for these uncertainties, we introduce three fitting parameters p, q_1 and q_2 to Equation 8:

$$\dot{V}(t) = \frac{-V(t)}{R_L C} - \frac{e_{31}W}{C}\left[h_{pc}\frac{d\theta(t)}{dt}\boldsymbol{p} - (s_1(t)-L)\frac{d\theta(t)}{dt}sin\theta(t)(\frac{\boldsymbol{q_1}}{R_L} + \boldsymbol{q_2})\right] \quad (9)$$

The values for p, q_1 and q_2 can be found for a given piezoelectric patch with the help of experimental measurements. In this work, we find the parameter values such that the normalized mean squared error between the experiments and model outputs are minimized:

$$Find \ p, q_1, q_2 \ such \ that \ \min_{p,q_1,q_2} \sum_{R_L} \frac{||V_{ref} - \hat{V}(p, q_1, q_2, R_L)||^2}{||V_{ref} - \frac{1}{N}\Sigma_{n=1}^{N}V_{ref}||^2} \quad (10)$$

where V_{ref} is the experimental voltage recording, $\hat{V}$ is the model voltage output given by Equation 9 and N is the number of samples in the experimental recording. This optimization problem is solved by the *fminsearch* function in MATLAB.

Finding the Generated Power: Once the output voltage is found by solving Equation 9, the voltage signal is used to compute the root-mean-square (RMS) voltage V_{RMS} and RMS power P_{RMS} as:

$$P_{RMS} = \frac{V_{RMS}^2}{R_L} \quad (11)$$

5 EXPERIMENTAL EVALUATION

Previous studies showed that the energy harvesting potential at knees is higher than than other joints due to higher torque at this location [11]. Thus, we choose the human knee as the target joint for validation and evaluate energy harvesting potential during walking.

5.1 Experimental Setup Design

Design & Fabrication: Reproducible and controlled experiments are crucial for a systematic validation study. To this end, we designed a mechanical frame that mimics the bending of the human knee joint, as shown in Figure 4-a. It is composed of the upper-leg, kneecap, lower-leg parts. The kneecap has a radius of curvature of 4 cm (r in Figure 3). Along all the three sections, a groove is present to place the piezoelectric patch for achieving good coupling to the motion. Also, screw holes are placed along the frame for mounting clampers to fix the piezoelectric patch. The frame is 3D printed using ABS plastic with 60% density for rapid prototyping.

Actuation: The frame is actuated through a Dynamixel AX-12A servo motor for controlled speed and angle. The motor is controlled through the dedicated OpenCM9.04 control board.

Placement: The piezoelectric patch is clamped to the lower-leg from one end, and is contained in the groove by a cover on the upper-leg as shown in Figure 4-b. The distance from the clamped end to curved surface is measured as 1.3 cm (s_0 in Figure 3). The
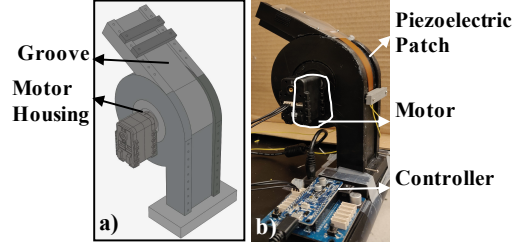

Figure 4: Mechanical human knee joint a) design in Solid-Works [16], b) 3D printed setup used in our experiments

other end of the piezoelectric patch is not clamped to avoid any extra strain caused by pulling of the material. In addition, extra care has been taken in order not to apply pressure onto the piezoelectric patch along the frame to avoid additional forces due to friction.

The rest of the setup consists of a variable resistance box for the load and NI DAQ for recording. We have a *companion ISLPED design contest submission* with this experimental setup.

5.2 Experimental Methods and Procedure

Piezoelectric Materials: We validate the proposed models using two different MFC patches: MFC85**28**P2 (the larger patch) and MFC85**14**P2 (the smaller patch) [17] as summarized in Table 3.

Excitation Input: We use four different sinusoidal excitation with the following bending angle and frequency pairs: (60°; 0.5 Hz), (60°; 1 Hz), (90°; 0.5 Hz), and (90°; 1 Hz). For example, the pair (60°; 0.5 Hz) means that the knee bends by 60° degrees starting from a neutral position and the movement is repeated with a frequency of 0.5 Hz. For each input, the angle is recorded with a Bendlabs sensor [18] to verify that the actuation follows the input excitation.

Load: We sweep the load connected to the MFC patches from 100 kΩ to 2MΩ for each input excitation. The load is incremented by 100 kΩ from 100 kΩ to 1 MΩ, and by 200 kΩ after that. The generated voltage for each value is recorded for ten seconds with NI DAQ.

Experiment Duration: To eliminate human related errors, all experiments have been repeated twice. Therefore, a total of 16 experiments (4 angle-frequency pairs × 2 MFC patches × 2 sets of measurements) are carried out *for each load value*. Each experiment takes approximately four hours with post-processing the recorded waveforms, which includes phase aligning the time series data to have zero initial condition and organizing the dataset. Hence, the measurements used in this study took about 64 man-hours.

5.3 Validation Under Controlled Experiments

The proposed model predicts the generated voltage as a function of time. Then, the output voltage is used to compute the generated power, which is the primary output. Therefore, we first summarize the accuracy in generating the output voltage and then present the accuracy in modeling the generated power in detail.

5.3.1 Output Voltage Comparison. As a representative example, Figure 5 shows the experimental voltage recording and the corresponding model output obtained with MFC8528P2 for (90°; 1 Hz) excitation and 0.4 MΩ load. The fitting parameters that minimize the error are found according to Equation 10. The model output closely follows the experimental voltage signal and achieves 2.7%

Table 3: Geometrical and physical parameters of the MFC patches used in our experimental validation.

	W (mm)	C (nF)	L (mm)	h_p (μm)	Y_p (GPa)	h_s (μm)	Y_s (GPa)	d_{31} (pC/N)	r (cm)	s_0 (cm)
MFC8528P2	28	264±20%	85	180	30.336	120	2.8	-170	4	1.3
MFC8514P2	14	138±20%								

mean absolute percentage error (MAPE). In general, the MAPE of the proposed model ranges from 0.78% to 3.6% for all experiments.

5.3.2 Output Power Comparison. Next, we analyze the generated power P_{RMS} in detail as a function of all input parameters and the load. Figure 6 plots the measured P_{RMS} and model results obtained from MFC8528P2. The MAPE of the proposed model is 5.4% and 5.3% for (90°; 1 Hz) and (60°; 1 Hz) input excitations, respectively (Figure 6-a). Similarly, it achieves 4.1% and 4.0% MAPE for (90°; 0.5 Hz) and (60°; 0.5 Hz) input excitations, respectively.

The validation results for MFC8514P2 (the smaller patch) are shown in Figure 7. When the patch swings at 1 Hz frequency, the proposed model achieves 3.6% and 1.5% MAPE for 90° and 60° bending angles, respectively (Figure 7-a). The corresponding errors at 0.5 Hz frequency are found as 6.9% and 3.8%, respectively. When all cases are considered together, *the average MAPE of the proposed model is 4.8%*. We draw three key observations from these results:

The bending angle only affects the magnitude of the generated power and does not shift the maximum power point (MPP). For example, Figure 6-a shows that for MFC8528P2, the MPP is at 0.4 MΩ for both (90°; 1 Hz) and (60°; 1 Hz). Similar behavior is observed for MFC8514P2 as shown in Figure 7. In all cases, the MPP predicted by the proposed model closely follows the measurements.

The excitation frequency affects both the magnitude and the optimum load, i.e., MPP. For instance, the MPP shifts from 0.4 MΩ to 0.8 MΩ and generated power drops nearly by half, when the excitation frequency decreases from 1 Hz to 0.5 Hz, as shown by Figure 6-a and Figure 6-b. This observation is expected and aligned with the first order approximation of a piezoelectric patch as a capacitance. In an RC circuit, maximum power transfer occurs at $R=\frac{1}{2\pi fC}$. Therefore, R is inversely proportional to both the excitation frequency and the capacitance of the piezoelectric patch.

Size of the piezoelectric patch also affects both the magnitude and the load value for the MPP. Smaller size yields less power, which is due to smaller piezoelectric material volume, hence, smaller dielectric displacement. Since the capacitance of the smaller patch is less, the MPP also shifts to higher load values. For example, when Figure 6-a and Figure 7-a are considered, going from the larger MFC8528P2 to the smaller MFC8514P2 shifts the MPP from 26 μW at R_L=0.4 MΩ to 14.7 μW at R_L=0.8 MΩ. This is expected since the maximum power transfer occurs at $R=\frac{1}{2\pi fC}$, as noted above.
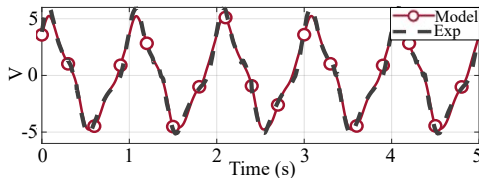

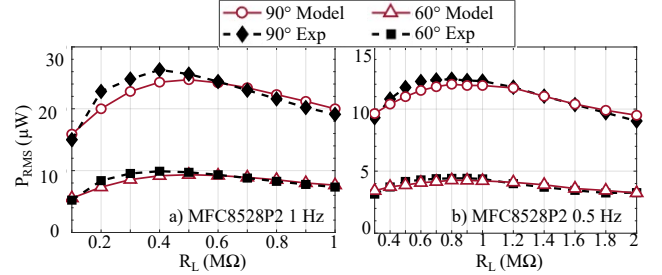**Figure 5: Voltage output of MFC8528P2. Input: 90° bending angle, 1 Hz excitation frequency. Load: R_L = 0.4 MΩ**

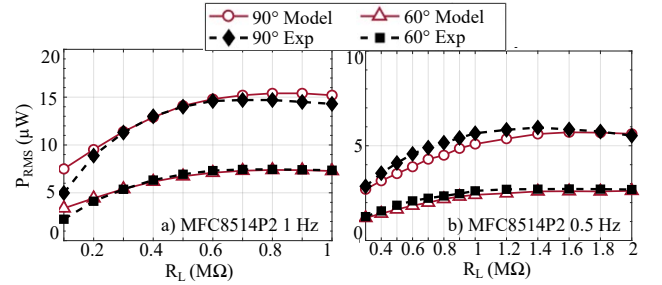**Figure 6: P_{RMS} for MFC8528P2 a) 1 Hz b) 0.5 Hz**

Figure 7: P_{RMS} for MFC8514P2 a) 1 Hz b) 0.5 Hz

5.4 Applications to Real Life Scenarios

This section illustrates the application of the proposed methodology to real-life scenarios. To this end, we recorded the knee angle of a user during walking using a bend sensor [18], shown in Figure 8-a. The bending angle is close to 60° and frequency is slightly less than 1 Hz. We consider MFC8528P2 as the piezoelectric patch and its maximum power point for 1 Hz excitation, i.e., R_L=0.4 MΩ, to analyze the harvesting potential. The recorded angle is fed as input to the proposed model to find the output voltage. The generated voltage leads to 6.5 μW RMS power. Considering both knees, we argue that 13 μW can be harvested by this user while walking.

Next, we investigate the use of the proposed approach in wearable applications. Let the duty ratio be the percentage of time a device can be powered by harvested energy. Figure 8-b shows the duty ratio for a hypothetical device spanning [1 μW, 1 mW] power consumption interval. If a device consumes less than 13 μW, PEH can power it perpetually, while devices with larger power consumption must turn off periodically. For example, the device presented in [19] consumes 137 μW; hence it can be powered with 9.4% duty cycle. To provide further insight, Figure 8-b shows the duty ratios for three wearable application examples from the literature [19–21].

Finally, we analyze the cumulative energy harvested by a person as a function of number of steps. Since each step takes around 1.2 seconds (Figure 8-a), 7.8 μJ of energy is harvested per step. Figure 8-c shows the distribution of the number of steps taken by an average person in the US [22] (right axis) and the equivalent battery capacity (left axis). As an example, a person who takes 7500 steps a day can produce $7500 \times 7.8 \times 30$=1.75 J in a month. This corresponds to 0.40 mAh battery charge capacity rated at 1.2V over a month.
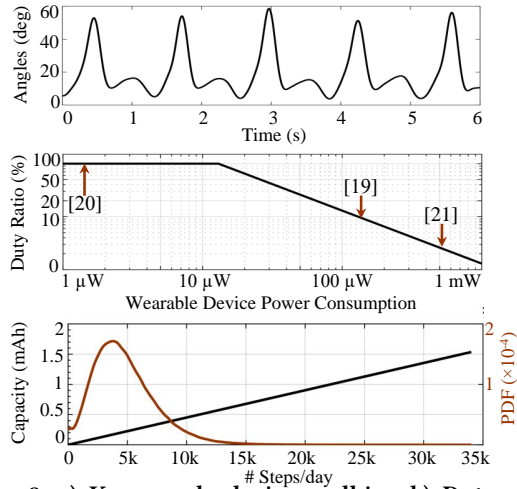
Figure 8: a) Knee angle during walking b) Duty ratio c) Charge capacity

6 CONCLUSION AND FUTURE WORK

Piezoelectric energy harvesting is an attractive solution for wearable devices. However, wearable PEH studies in the literature are usually bulky and impractical. In this paper, we present a mathematical model for flexible patches placed directly on joints and validate it through experimental evaluations for the first time. Once its validity is established, we use the proposed model to project the energy harvesting potential from walking. According to our results, 13 μW can be harvested from the knees during walking.

In this work, we used two excitation frequencies (0.5 Hz and 1 Hz) and two bending angles (60° and 90°) for validation. As future work, we will extend the validation set to achieve a finer granularity that can capture different walking patterns. We plan to also apply the proposed technique to other piezoelectric materials. Finally, we plan to improve the proposed technique by investigating the effect of fitting parameters and simplifying the model.

ACKNOWLEDGMENTS

REFERENCES
[1] Y. Khan *et al.*, "Flexible Hybrid Electronics: Direct Interfacing of Soft and Hard Electronics for Wearable Health Monitoring," *Advanced Functional Materials*, vol. 26, no. 47, pp. 8764–8775, 2016.
[2] M. Bariya, H. Y. Y. Nyein, and A. Javey, "Wearable sweat sensors," *Nature Electronics*, vol. 1, no. 3, pp. 160–171, 2018.
[3] H. Jeong *et al.*, "Modular and reconfigurable wireless e-tattoos for personalized sensing," *Adv. Mater. Technol.*, vol. 4, no. 8, p. 1900117, 2019.
[4] Wired, "The future of wearable tech," Online, 2015, https://www.wired.com/insights/2015/02/the-future-of-wearable-tech/, accessed 28 Feb 2020.
[5] P. D. Mitcheson, E. M. Yeatman, G. K. Rao, A. S. Holmes, and T. C. Green, "Energy harvesting from human and machine motion for wireless electronic devices," *Proceedings of the IEEE*, vol. 96, no. 9, pp. 1457–1486, 2008.
[6] S. Sudevalayam and P. Kulkarni, "Energy harvesting sensor nodes: Survey and implications," *IEEE Commun. Surv*, vol. 13, no. 3, pp. 443–461, 2010.
[7] H. Kulah and K. Najafi, "Energy scavenging from low-frequency vibrations by using frequency up-conversion for wireless sensor applications," *IEEE Sensors Journal*, vol. 8, no. 3, pp. 261–268, 2008.
[8] M. Pozzi and M. Zhu, "Plucked piezoelectric bimorphs for knee-joint energy harvesting: modelling and experimental validation," *Smart Materials and Structures*, vol. 20, no. 5, p. 055007, 2011.
[9] Y. Kuang, Z. Yang, and M. Zhu, "Design and characterisation of a piezoelectric knee-joint energy harvester with frequency up-conversion through magnetic

plucking," *Smart Materials and Structures*, vol. 25, no. 8, p. 085029, 2016.
[10] H. Liu, J. Zhong, C. Lee, S.-W. Lee, and L. Lin, "A comprehensive review on piezoelectric energy harvesting technology: Materials, mechanisms, and applications," *Applied Physics Reviews*, vol. 5, no. 4, p. 041306, 2018.
[11] A. Proto, M. Penhaker, D. Bibbo, D. Vala, S. Conforto, and M. Schmid, "Measurements of generated energy/electrical quantities from locomotion activities using piezoelectric wearable sensors for body motion energy harvesting," *Sensors*, vol. 16, no. 4, p. 524, 2016.
[12] G. Bassani, A. Filippeschi, and E. Ruffaldi, "Nonresonant kinetic energy harvesting using macrofiber composite patch," *IEEE Sensors Journal*, vol. 18, no. 5, pp. 2068–2076, 2018.
[13] Y. Cha, "Energy harvesting using flexible piezoelectric materials from human walking motion: Theoretical analysis," *Journal of Intelligent Material Systems and Structures*, vol. 28, no. 20, pp. 3006–3015, 2017.
[14] A. Erturk and D. J. Inman, "A Distributed Parameter Electromechanical Model for Cantilevered Piezoelectric Energy Harvesters," *Journal of Vibration and Acoustics*, vol. 130, no. 4, 2008.
[15] N. G. Elvin and A. A. Elvin, "Large deflection effects in flexible energy harvesters," *J INTEL MAT SYST STR*, vol. 23, no. 13, pp. 1475–1484, 2012.
[16] Solidworks, *2019*. Waltham, Massachusetts: 3DS, 2019.
[17] "Mfc p2 and p3 types," https://www.smart-material.com/MFC-product-P2.html.
[18] Bend Labs, "Flexible Single Axis Bidirectional Sensor," 2019, [Online] https://www.bendlabs.com/products/1-axis-evaluation-kit/, accessed 26 Nov. 2019.
[19] T. Yoo, J. E. Kim, N. Le Ba, K.-H. Baek, T. T. Kim *et al.*, "A 137-μw area-efficient real-time gesture recognition system for smart wearable devices," in *IEEE A-SSCC*, 2018, pp. 277–280.
[20] X. Zhang, Z. Zhang, Y. Li, C. Liu, Y. X. Guo, and Y. Lian, "A 2.89μw dry-electrode enabled clockless wireless ecg soc for wearable applications," *IEEE journal of solid-state circuits*, vol. 51, no. 10, pp. 2287–2298, 2016.
[21] S. Kang, J. Lee, K. Bong, C. Kim, and H.-J. Yoo, "A 0.53 mw ultra-low-power 3d face frontalization processor for face recognition with human-level accuracy in wearable devices," in *IEEE ISCAS*, 2017, pp. 1–4.
[22] T. Althoff, J. L. Hicks, A. C. King, S. L. Delp, J. Leskovec *et al.*, "Large-scale physical activity data reveal worldwide activity inequality," *Nature*, vol. 547, no. 7663, pp. 336–339, 2017.

A APPENDIX A

To evaluate the integral in Equation 7, the first term is divided into three regions $[0, s_0]$, $[s_0, s_1]$ and $[s_1, L]$ along the length of the patch:

$$\int_0^L -h_{pc}\kappa(s,t)ds =$$

$$\int_0^{s_0} -h_{pc}\kappa(s,t)ds + \int_{s_0}^{s_1} -h_{pc}\kappa(s,t)ds + \int_{s_1}^{L} -h_{pc}\kappa(s,t)ds \quad (12)$$

Here, the first and third integrals evaluate to 0 as $\kappa(s,t) = 0$ in those intervals. The middle integral is evaluated as:

$$\int_{s_0}^{s_1} -h_{pc}\kappa(s,t)ds = \int_{s_0}^{s_0+r\theta(t)} -h_{pc}\frac{1}{r}ds = -h_{pc}\theta(t) \quad (13)$$

The second term in Equation 7 is readily integrable as:

$$\int_0^L \frac{\partial u(s,t)}{\partial s}ds = u(L,t) - u(0,t) \quad (14)$$

From (2), $u(0,t) = 0$. With these, Equation 7 reduces to:

$$Q(t) = -CV(t) + e_{31}W\left(-h_{pc}\theta(t) + u(L,t)\right) \quad (15)$$

Next, we take the time derivative of $Q(t)$ to obtain the electrical current generated by the piezoelectric patch:

$$i(t) = \frac{dQ(t)}{dt} = -C\frac{dV(t)}{dt} + e_{31}W\left(-h_{pc}\frac{d\theta(t)}{dt} + \frac{du(L,t)}{dt}\right) \quad (16)$$

From (2), we obtain $\frac{du(L,t)}{dt} = (s_1(t) - L)\frac{d\theta(t)}{dt}sin\theta(t)$. Then, from $V(t) = i(t)R_L$, we get the differential equation that describes the voltage as:

$$\frac{dV(t)}{dt} = \frac{-V(t)}{R_L C} + \frac{e_{31}W}{C}\left(-h_{pc}\frac{d\theta(t)}{dt} + (s_1(t) - L)\frac{d\theta(t)}{dt}sin\theta(t)\right) \quad (17)$$